

Raman spectroscopy coupled to computational approaches towards understanding self-assembly in thermoreversible poloxamer gels

Michael T. Cook, Mohamad A. Abou-Shamat, Jacqueline L. Stair and Jesus Calvo-Castro\*

*School of Life and Medical Sciences, University of Hertfordshire, Hatfield, AL10 9AB, UK  
E-mail: j.calvo-castro@herts.ac.uk.*

Keywords: poloxamers, pluronics, kolliphors, Raman spectroscopy, chemometrics, quantum mechanics

### **Abstract**

The exploitation of vibrational spectroscopy approaches towards the understanding of molecular-level events in polymers, such as poloxamers, is highly warranted. This would facilitate the development of real-time approaches to monitor processes as well as the rational realisation of superior architectures. To date, studies on poloxamer based materials are restricted to low concentration materials and the evaluation of vibrational frequencies involving C-H stretching motions. We carry out an in-depth analysis of thermally-induced micellization processes employing technologically relevant 20% w/w P407 aqueous formulations. Our results, coupling Raman spectroscopy to computational approaches, are unequivocally consistent with such temperature-controlled events not being restricted to molecular re-arrangements involving C-H stretching motions. In fact, the synergistic approach of all key spectral regions was observed to yield optimum delineation of formulations at different temperatures. Vibrational envelopes were deconvoluted and it was observed that vibrational analysis of convoluted spectra can often be misleading. Individual contributions were assigned to either PEO or PPO building blocks by means of quantum-mechanical calculations. Temperature-induced changes to both intensity and vibrational frequencies were statistically evaluated and identified variations rationalised based on intermolecular interactions and structural order/disorder of the polymer units. Such observations were identified to be critically different depending on the nature of the vibrations.

## 1. Introduction

Thermoreversible gels undergo a reversible transformation from liquid to gel with temperature and are typically aqueous polymer solutions.<sup>[1]</sup> These materials have been drawing attention for numerous applications such as drug delivery,<sup>[2]</sup> wound dressings,<sup>[3]</sup> bio-printing<sup>[4]</sup> and tissue engineering.<sup>[5]</sup> Among the different thermoresponsive materials that have been exploited is poloxamer 407 (P407), a poly(ethylene oxide)<sub>101</sub>-poly(propylene oxide)<sub>65</sub>-poly(ethylene oxide)<sub>101</sub> (PEO-PPO-PEO) triblock copolymer (Figure 1).<sup>[6]</sup> The liquid-like properties of P407 below the temperature of gelation ( $T_{gel}$ ) are ideal for ease of handling, allowing processes such as extrusion, mixing or spraying. When heated to  $T_{gel}$  the solution transitions to a gel state, which can be triggered by the body's heat for pharmaceutical exploitation, for example as an *in situ* gel.<sup>[7,8]</sup> Furthermore, the polymer is chemically stable and has been approved by the Food and Drug Administration (FDA) as an excipient for multiple drug formulations.<sup>[6]</sup> This has led to P407 being investigated in combination with polymer additives to develop complex formulations for drug delivery.<sup>[1,9,10]</sup>

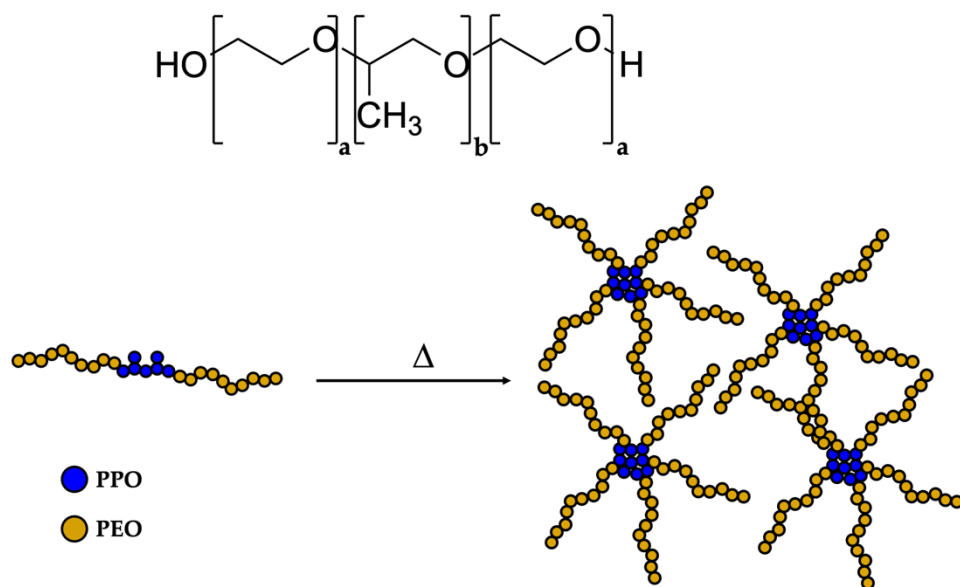


**Figure 1.** Schematic chemical structure of P407 (top,  $a = 101$  and  $b = 65$ ) and illustration of the micellization in this material as a function of temperature (bottom).

Despite the aforementioned technological relevance of poloxamer-based thermoresponsive materials, there remains a highly warranted need to acquire a more in-depth understanding of the thermally-induced gelation mechanism in these materials. This would not only lead to the optimization of manufacturing processes but also inform the rational design of superior

formulations to those currently being exploited. By means of nanostructural characterization techniques such as temperature transmission electron microscopy (cryo-TEM),<sup>[11]</sup> small angle neutron scattering (SANS)<sup>[12,13]</sup> and dynamic light scattering (DLS),<sup>[11]</sup> it is currently accepted that the gelation mechanism for P407 results from the dehydration of the PPO block constituting the central “B” block in the poloxamer ABA structure.<sup>[8]</sup> At low temperatures below the critical micellization temperature (CMT), both the PEO and PPO block are hydrated, and the PPO block is to some extent soluble in water.<sup>[11]</sup> With an increase in temperature, the PPO block becomes less water-soluble, micelles start to form with a core of hydrophobic PPO and corona of hydrophilic PEO, and their volume fraction increases. At a critical volume fraction ( $> 0.53$ ),<sup>[14,15]</sup> micelles become arrested and immobile, forming a liquid crystalline phase which leads to the solution transitioning to a gel.<sup>[14]</sup>

Vibrational spectroscopy approaches have been exploited in adding further discrimination at molecular-level events in these technologically relevant materials, such as desolvation, conformational changes and intermolecular interactions.<sup>[13,16,17]</sup> Along those lines, Guo et al. investigated thermally-induced phase transitions in 10% (w/w) aqueous solutions of P407 analogues with varying PPO/PEO ratios ( $P407_{PPO/PEO} = 0.32$  for reference), namely P103 (1.79), P104 (1.15), P105 (0.76) and F88 (0.19) as well as neat PEO and PPO for comparison using Raman spectroscopy.<sup>[18,19]</sup> In their work, they demonstrate that micellization-induced gelation in these materials results in noticeable changes to both intensity and frequency of symmetric as well as asymmetric C-H stretching vibrational motions in the 2800-3000  $\text{cm}^{-1}$  spectral region. Through spectral deconvolution of this vibronic envelope, they tentatively associated individual contributions to either PEO or PPO blocks and rationalized structural changes as a consequence of phase transitions to solvation/desolvation events. In short, it was proposed that when the polymers are hydrated at temperatures below  $T_{\text{gel}}$ , the frequencies of these vibrational modes shift to higher frequencies due to interaction with water molecules. As the temperature increases, particularly above  $T_{\text{gel}}$ , these frequencies decrease again. This was observed to be more significant in the case of signals associated to PPO blocks due to their hydrophobic nature and central location in the micelle structure. This was also associated to an increase in the order of the PPO units, unlike the outer PEO blocks which transition to more disordered arrangement as a consequence of the increase in temperature.

Whilst these studies have been valuable in contributing to the understanding of these thermally-induced processes in poloxamer formulations, they were limited to i) monitoring spectral changes associated to C-H stretching vibrational motions and ii) formulations characterized by arguably low concentrations (10% w/w). Along these lines, it would be of significant

technological interest the evaluation of higher concentration formulations capable of undergoing thermoreversible gelation ( $> 15\%$  w/w)<sup>[20]</sup> as well as the in-depth analysis of lower frequency spectral regions. We anticipate that the latter could facilitate the development of approaches for real-time monitoring of these temperature-controlled events by portable Raman instrumentation which often monitors spectral regions below  $2800\text{ cm}^{-1}$ . In addition, it is of particular concern to us that in most cases, the reported frequency shifts associated to the thermally-induced structural re-arrangements were smaller than their reported spectral resolution of  $4\text{ cm}^{-1}$ .<sup>[18]</sup>

Motivated by these shortcomings and the increasing interest in vibrational spectroscopic techniques to investigate microenvironmental and conformational changes in polymer solutions, herein we carry out a thorough study of the thermally-induced micellization process in 20% w/w P407 aqueous formulations by means of spectroscopic as well as computational approaches to unequivocally understand the contribution of the different building blocks. To the best of our knowledge this is the first report which investigates P407's micellization by means of Raman spectroscopy and computational approaches, highlighting that such temperature-controlled events are not restricted molecular re-arrangements involving C-H stretching vibrational motions. To do that we first evaluated the Raman spectral profile of P407 in the solid state as well as 20% (w/w) formulations as a function of temperature (10, 15, 20 and  $37\text{ }^{\circ}\text{C}$ ), comparing these to previous studies on structural analogues and rationalizing the observations based on the PPO/PEO ratios. We then subject our dataset to chemometric analysis by Principal Components (PCA). Our results indicate that i) micellization in these formulations may be seen as a shift in equilibria to gradually favour the micellar form, rather than a binary transition to an entirely micellar state – which was further confirmed by means of rheological as well as DLS analyses and ii) contrary to previous reports, observed scores plot delineation and associated loading plots are consistent with conformation changes not solely limited to the C-H stretching spectral region. Next, we dedicate the remaining of this work to the in-depth investigation of the micellization-induced structural re-arrangements in P407 aqueous solutions. To do that, each of the five key spectral regions that were previously identified was subjected to spectral deconvolution and individual deconvoluted signals were assigned to either PEO or PPO by means of quantum-mechanical calculations. Their vibrational frequencies and relative intensities were subjected to statistical analyses and observed changes rationalized based on intermolecular interactions and structural order/disorder of the polymer as a function of temperature, respectively. As a result, we strongly believe this study to be of interest for the

increasingly large scientific community devoted to the investigation of micellization processes in thermoreversible polymeric materials and their technological applications.

## 2. Experimental Section

### *Dynamic Light Scattering:*

A sample of 1 mL of P407 (Merck, UK – used as supplied) solution (10 mg/mL) in deionised water was prepared and filtered using a syringe filter (0.22  $\mu\text{m}$ ). Dynamic Light Scattering (DLS) was then conducted using a Malvern Zetasizer Nano ZS with a scattering angle of  $173^\circ$  and attenuator set at 8 (3 % beam transmission). The scattering intensity of the sample was measured between 10 and 40  $^\circ\text{C}$ , where an increase in the intensity of scattered light is assumed to be related to the formation of nanodimensional micelles.

### *Raman spectroscopy:*

Samples interrogated by Raman spectroscopy were prepared following a modified version of the cold method reported by Schmolka.<sup>[21]</sup> Briefly, 4 g of P407 was added gradually to 6 g of distilled water and 10 g of 0.02 M phosphate buffered solution while stirring in an ice bath. The solution was then left in the bath with stirring for one hour before moving to the refrigerator overnight at 4  $^\circ\text{C}$  prior to analysis. Raman analyses were carried out employing a benchtop Renishaw inVia Raman microscope equipped with a high sensitivity ultralow noise RenCam CCD detection and ultra-high precision diffraction grating of 1200 lines/mm, with a resolution of 0.6  $\text{cm}^{-1}$ . The instrument was operated using the WiRe software supplied by the manufacturer. In all cases, reported spectra were acquired utilising a 785 nm excitation wavelength with a ca 5.8 mW power at sample, and a spectral range of 100-3200  $\text{cm}^{-1}$ . Samples were presented to the Raman microscope on aluminium foil on top of a THMS600 Linkam temperature-controlled stage. Temperature at the sample was monitored continuously using a thermocouple, with negligible changes to the integrity of the samples observed upon irradiation. For each evaluated temperature (10, 15, 20 and 37  $^\circ\text{C}$ ), samples were interrogated 20 times, focusing on different sample areas in order to account for any possible anisotropic effects.

### *Rheometry:*

Rheology experiments were performed using a TA instruments AR 1500 ex rheometer fitted with a solvent trap using a 40 mm parallel plate geometry with a 600  $\mu\text{m}$  gap. The samples were left to equilibrate for 5 min at 15  $^\circ\text{C}$  on the rheometer peltier plate. Then temperature ramp measurements were carried out at a frequency of 1 Hz and oscillatory stress of 1 Pa, with temperatures increased at a rate of 1  $^\circ\text{C min}^{-1}$ .

### *Principal Component Analysis:*

Experimental Raman spectra ( $n = 20$ ) for each evaluated temperature were subjected to chemometric analyses by Principal Component Analysis (PCA), employing NIPALS (Non-linear Iterative Projection by Alternating Least Squares) algorithm as implemented in the Unscrambler X 10.5.1 software. All generated PCA models were full cross validated (one sample per segment).

#### *Computational methods:*

The geometry of a representative P407 enneadecamer (7:5:7) was optimised, without imposing any constraints, employing the B3LYP density functional<sup>[22–24]</sup> at the 6-31G(d) level as implemented in Spartan '20 (version 1.1.1).<sup>[25]</sup> The optimised geometry was then subjected to infrared analysis returning non-negative frequencies in all cases, thus consistent with a true equilibrium minimum.<sup>[26,27]</sup> Harmonic frequencies and Raman intensities were computed at the same level of theory, with observed scaling factor in line with those previous reported for the density functional of choice (e.g. 0.952).<sup>[28,29]</sup>

#### *Spectral deconvolution:*

Experimental Raman spectra were subjected to a spectral deconvolution protocol as implemented in OriginPro 2019b, employing the quadratic Savitzky-Golay algorithm.

#### *Statistical analysis:*

Changes to vibrational frequencies and intensities for each individual (deconvoluted) signal were statistically evaluated for differences by means of one-way analysis of the variance (ANOVA) and post-hoc Tukey's test to investigate all possible pairwise comparisons for these formulations at the different temperatures. In all cases 0.05 was used as the significance level ( $p$ ), with results characterised by  $p < 0.05$  being considered as statistically different.

### **3. Results and Discussion**

#### **3.1 Raman spectroscopy and phase transition of thermoreversible P407 gel**

We first started by evaluating the spectral properties of P407 in the powder form by Raman spectroscopy and carry out a comparison with other structural analogues with different PPO/PEO ratios.<sup>[18]</sup> As illustrated in **Figure 2**, the Raman spectrum of P407 is characterized by clearly defined vibrational bands centred at ca 280, 843, 1143, 1281, 1482 and 2891  $\text{cm}^{-1}$ , with the first of these associated to low frequency longitudinal acoustic modes. It should be noted that in the following we based our in-depth analysis on vibrational envelopes characterized by frequencies larger than those of acoustic modes.<sup>[18,30]</sup> These higher frequency modes can be broadly associated to C-O-C stretching motions (843 and 1143  $\text{cm}^{-1}$ , highly coupled to C-H rocking motions in the case of the latter), C-H wagging and rocking motions (1281  $\text{cm}^{-1}$ ), C-H

bending ( $1482\text{ cm}^{-1}$ ) and C-H stretching ( $2891\text{ cm}^{-1}$ ) and for simplicity will be referred to in this manuscript as A-E key spectral regions, respectively. For the C-H stretching region (E), which has been widely employed previously in the study of these thermally-induced processes, we observed the appearance of a second maximum, of comparable intensity to the first one, on progression to the solubilised polymer. This second maximum, centred at ca  $2940\text{ cm}^{-1}$ , is characterized by two equally intense inflections at  $10\text{ }^{\circ}\text{C}$  and further exhibits a progression to higher frequencies as the temperature of the formulations is increased. In turn, a shift to lower frequencies is observed to the other maximum in the progression as the temperature is increased. These significant changes to the E spectral region are consistent with the higher PEO than PPO content in P407 and have been previously observed for structural analogues with small PPO/PEO ratios such as F88.14<sup>[31]</sup>

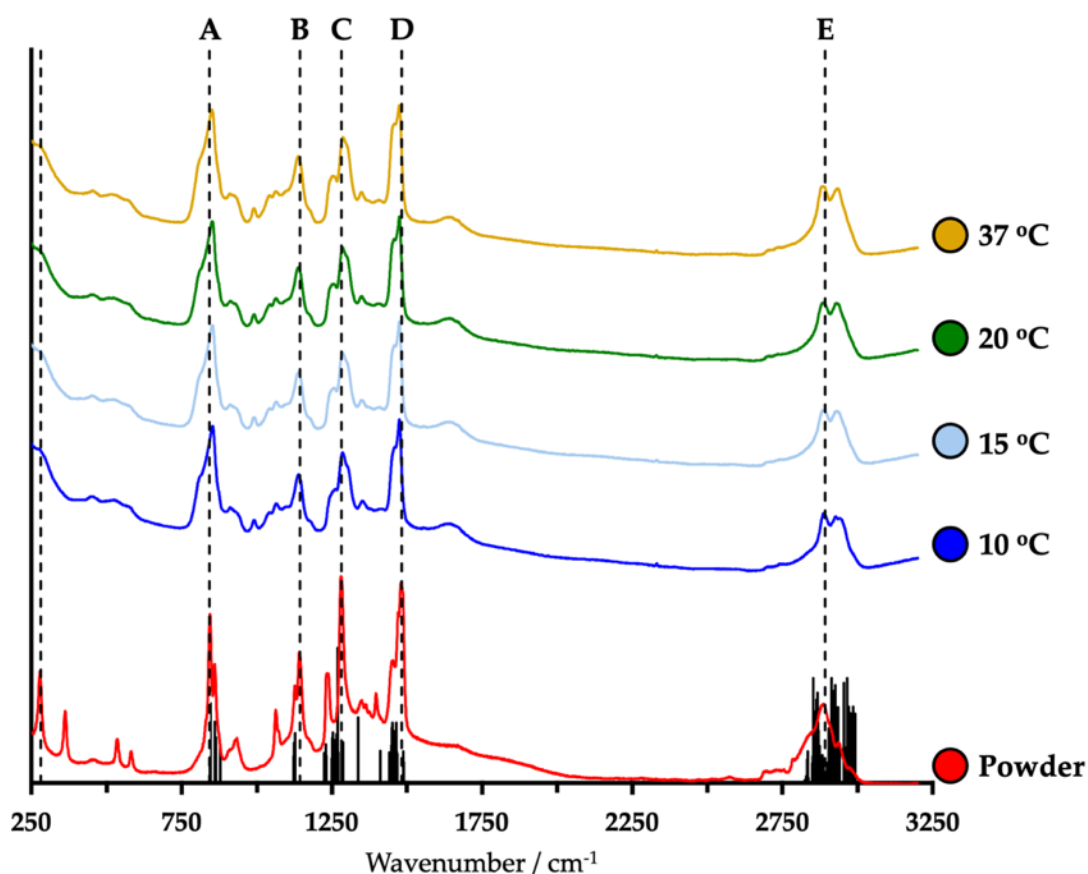


**Figure 2.** Normalised and offset Raman spectra of powder P407 (red solid line) and aqueous formulations at 10 (light blue solid line), 15 (dark blue solid line), 20 (green solid line) and 37 °C (yellow solid line). Vertical black dashed lines illustrate the position of the centre of the main bands in the spectrum of the powder. Vertical black lines illustrate the harmonic vibrational frequencies at B3LYP/6-31G(d)//B3LYP/6-31G(d) computed for a representative

P407 enneadecamer (7:5:7). Scaling factor,  $s = 0.952$ .<sup>[28,29]</sup> Figure 5-9 illustrate key spectral regions A-E, respectively.

Irrespective of the spectral region, progression from anhydrous polymer to low (10 °C) temperature solution is consistent with these vibrational envelopes becoming broader and less resolved, which can be accounted for by means of an increase in the number of thermodynamically available P407 chain conformations afforded. This spectral broadening represents an added complexity when trying to evaluate the role played by specific polymer building blocks in those conformational changes at the molecular level. It could be anticipated that in such solvation processes, the vibrational frequencies for individual modes shift to higher frequencies as a result of intermolecular interactions between the polymer chains and water molecules. In this regard, visual inspection of the spectral signatures in **Figure 2** on progression from anhydrous to 20% w/w aqueous solution of P407 at 10 °C is consistent with clear spectral changes. However, it is observed that while the centre of the main bands in spectral regions A and C do shift to higher frequencies, the opposite behaviour is exhibited by vibrational envelopes in regions B and D. The latter observation is anticipated to result as a consequence of the synergistic changes to the position and/or relative intensity of the individual signals conforming the convoluted band and should not be taken as a spectral marker for these structural re-arrangements on progression to aqueous formulations. Further, it is of note the observed subtle changes to these vibronic progressions as the temperature of the formulation is increased, in line with the known thermally-induced micellization processes that these undergo. In light of these observations, we hypothesise that contrary to previous efforts, the utilisation of vibrational spectroscopic techniques for the understanding of these temperature-controlled processes should not be limited to changes in the C-H stretching vibrational motions and that other regions, namely A-D herein, should also be investigated in-depth. Thus, we next went on to critically assess the experimental Raman spectra of these aqueous formulations at different temperatures by means chemometric analysis by Principal Components (PCA), a multivariate technique that has previously been employed in the analysis of spectroscopic data.<sup>[32-34]</sup> For this analysis, the NIPALS (Non-linear Iterative Projection by Alternating Least Squares) algorithm was implemented in the Unscrambler X 10.5.1 software. Each generated model was full cross validated (one sample per segment).

The results of a PCA model are usually presented in a two- or three-dimensional plot, which is referred to as scores plot. Samples (or scores) are distributed across those plots according to the similarities in their variables (vibrational frequencies in this case). Each axis in the scores plots

is known as a principal component, accounting for a percentage of the total variance of the dataset and which is a linear combination of the variables where the coefficients are referred to as loadings. Given the large number of variables (3642), we explored systematic step-wise data reduction methodologies to identify the optimum spectral region of interest whilst maximising the amount of explained variance, particularly by the first two and three principal components which carry the majority of it. As such, five different PCA model systems, one per spectral region of interest (*vide supra*), were developed comprising 20 replicate spectra for each of the four evaluated temperatures. In short, we observed in all cases that data model systems generated for these individual regions were able to account for a large amount ( $\geq 90\%$ ) of explained variance by means of the first two principal components (**Figure S1.1-5**). However, we observed that clear delineation of the four subsets was not afforded by any of these model systems. Generated models for spectral regions A-D were able to delineate formulations at 37 °C from those at other temperatures, to a greater extent in the case of model systems for spectral regions B and C. In turn, the developed model for the widely employed region E was characterised by clearly delineated P407 aqueous formulations at 10 °C from those at other temperatures along the second principal component. Interestingly, subsets for 15, 20 and 37 °C were delineated along the first principal component, in line with a greater loading contribution for the signals at ca 2920  $\text{cm}^{-1}$ .

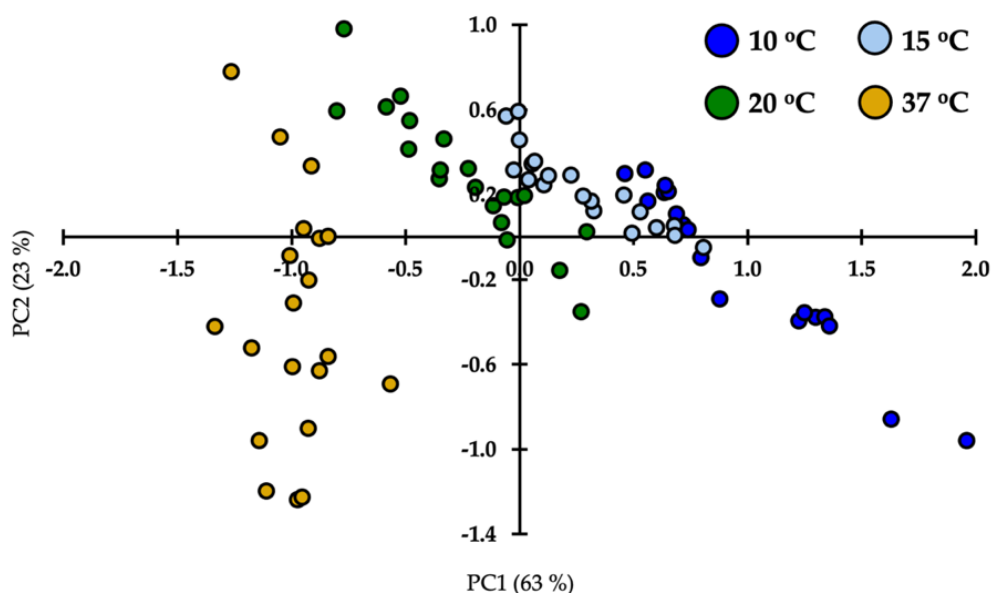


**Figure 3.** Two-dimensional scores plot generated using Raman spectra for P407 20% w/w aqueous formulations ( $n=20$ ) at different temperatures. Solid filled circles in light blue, dark blue, green and yellow denote scores for 10, 15, 20 and 37 °C.

To continue testing our hypothesis that the monitoring of molecular-level conformational changes in P407 aqueous formulations should not be solely restricted to changes affecting C-H stretching motions, a PCA model was generated employing the full spectral range, 100-3200  $\text{cm}^{-1}$  (**Figure 3**). Despite the significantly larger spectral range, the generated model was able to account for a comparable (89%) amount of explained variance using the two first principal components when compared to the individual model systems for each key spectral region. It is noteworthy the discriminative ability of the newly developed model, being able to delineate the scores for these aqueous formulations for all four different temperatures, unlike the individual model systems previously generated (**Figure S1.1-5**). Whilst model systems for these key spectral regions were able to delineate scores for lowest/highest temperatures with respect to the other ones, different regions were occupied by each subset in this full spectral range model system. Importantly, it was observed that these subsets were delineated primarily along the first principal component, which carries the largest amount of explained variance (63 and 23% explained variance by PC1 and 2, respectively). This contrasts with the observation made in all cases for individual models whereby the main delineation channel was denoted by the second and not the first principal component, which were characterised by arguably small amount of explained variance in some cases (e.g. 12 and 5% for PC2 in model systems for C and D spectral regions, respectively). As a result, we have demonstrated that the synergistic utilisation of all key spectral regions yields superior delineation performance in these PCA model systems when compared to individual ones.

Moreover, the relative delineation illustrated in **Figure 3** would be consistent with a gradual micellization process rather than a binary transition to an entirely micellar state. To further evaluate this observation, the behaviour of these aqueous formulations was evaluated using dynamic light scattering (DLS) and rheology. DLS analyses were conducted as a temperature ramp measuring scattering of a 10 mg/mL P407 solution in water. **Figure 4** (left) illustrates the mean count rate, indicating the average scattering intensity during the measurement, as a function of temperature. This is consistent with an increase in the count rate at ca 22 °C, which can be ascribed to the formation of scattering micelles. In short, this count rate is related to the number of scattering particles in solution. It is now accepted that P407 aqueous solutions form spherical micelles over a wide range of temperatures above the critical micelle temperature (CMT). This is in agreement with the scores plot in **Figure 2**, reinforcing that this thermally-induced transition can be interpreted as a gradual shift in equilibrium rather than a sudden onset. To further support these observations, a rheometric small-amplitude oscillatory temperature

ramp experiment was conducted in 20% w/w aqueous solutions of our poloxamer of interest, P407. As illustrated in **Figure 4** (right), these formulations exhibit lower storage ( $G'$ ) than loss ( $G''$ ) moduli values at temperatures below ca 15.8 °C, hence consistent with a liquid-like behaviour. In turn, as the temperature is increased the storage modulus is observed to increase more rapidly than the loss modulus, which is consistent with an elastic behaviour of the material.<sup>[35][36]</sup>

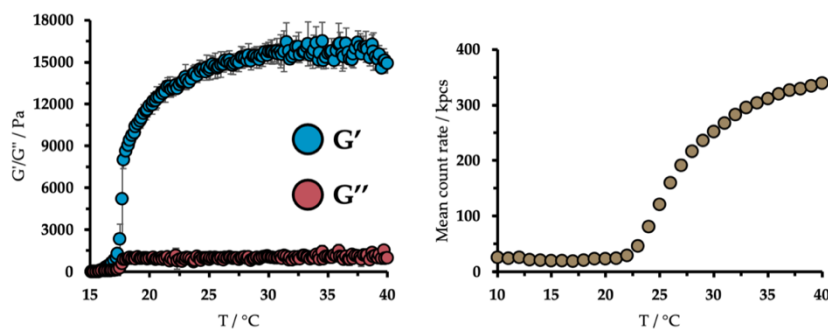


**Figure 4.** Oscillatory rheology (1 Pa, 1 Hz) of a 20 % w/w aqueous solution of P407 as a function of temperature (left) and scattered light from a 10 mg/mL P407 solution in water as measured by dynamic light scattering (right).

To further understand these observations from the chemometric analysis of the thermally-induced gelation of these P407 aqueous formulations, we analysed the generated line loadings for the two principal components. Where the modulus of the loading indicates the relevance of that variable (vibrational frequency) in explaining the variance of the dataset. In both cases, we observed particularly high loadings in spectral regions which coincide with those previously referred to as key by us (**Figure S2.1-6**). These results would be consistent with the observed delineation and proposed conformational changes being associated with simultaneous subtle yet significant spectral differences as a function of temperature, and not isolated contributions from one of the key spectral regions previously defined. In light of the intrinsically broad nature of these spectral signatures in the Raman spectra of P407 20% w/w aqueous formulations, we deemed it necessary to deconvolute these complex vibronic envelopes into their individual components, with a view to unequivocally identify spectral vectors for these thermally-controlled structural re-arrangements.

**3.2 Spectral deconvolution and conformation changes.** In line with the Raman spectral features of these formulations and further supported by the findings from the chemometric

analyses by principal components, the vibrational features on these five different key spectral regions will be investigated in-depth. To do this, each of these complex envelopes was deconvoluted into their individual components. Subsequently, these individual signals were unequivocally assigned to functional groups in P407 aided by quantum mechanical calculations on an optimised P407 representative enneadecamer (**Table S3.1**). Changes to both intensity and frequency for each individual vector as a function of temperature was statistically evaluated by means of one-way analysis of the variance (ANOVA) and subsequently subjected to a post-hoc Tukey's test to investigate all possible pairwise comparisons for these formulations at the different temperatures.

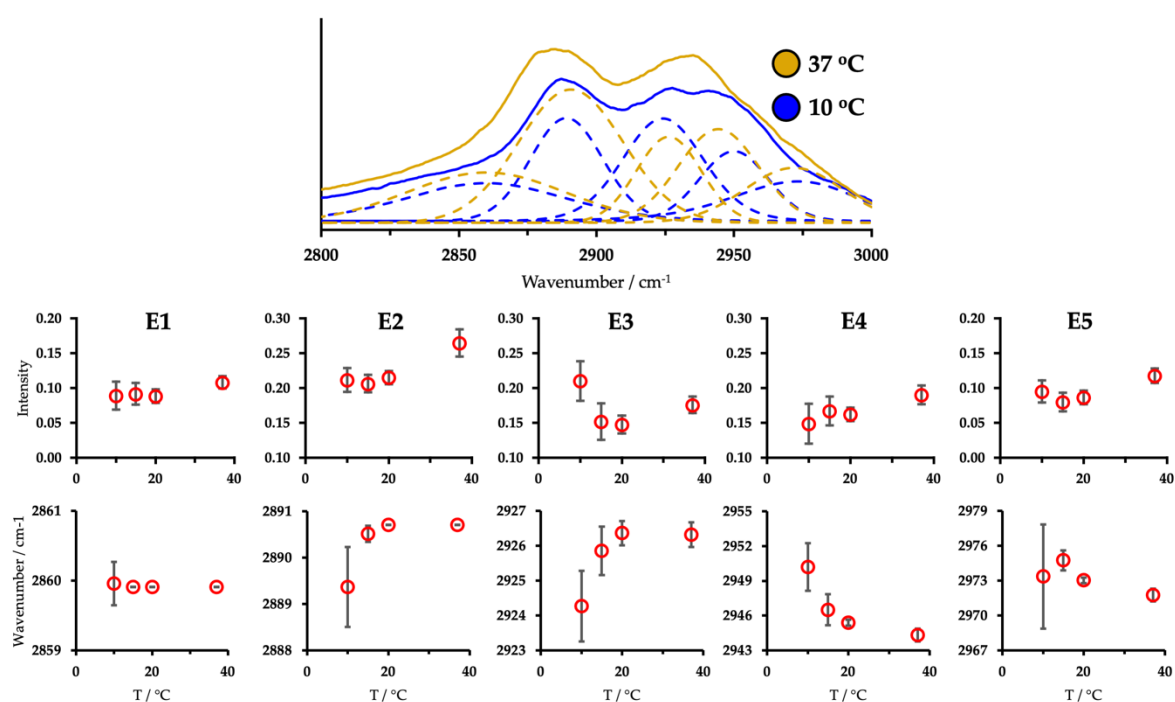


**Figure 5.** Raman spectra of 20% w/w aqueous formulations of P407 at 10 (blue solid line) and 37 °C (yellow solid line), including deconvoluted bands (illustrated as dotted lines) for the E spectral region (2800-3020 cm<sup>-1</sup>). Two dimensional Figures illustrate the changes to intensities (top) and vibrational frequencies (bottom) as a function of temperature for all deconvoluted signals (grey solid lines illustrate the associated uncertainties as standard deviations).

Given that previous studies on P407 structural analogues have solely restricted their analysis to those vibrational motions associated to C-H stretching in the herein referred to as key spectral region E, we devote the first part of this subsection to the spectral signatures resulting from these vibrational motions. On comparison with other key spectral regions (vide infra), this one

is certainly characterised by exhibiting the greatest complexity alongside region B. As a result, spectral deconvolution and computational band assignment was deemed as critical. This complex envelope was successfully deconvoluted into five different Gaussian peaks, namely E1-5 centred at ca 2859, 2889, 2925, 2946 and 2972  $\text{cm}^{-1}$ , respectively. These were associated to both symmetric and asymmetric C-H stretching vibration. Aided by computational approaches, we were able to associate all five bar E2-3 to poloxamer's PPO segments. **Figure 5** illustrates these deconvoluted signals at both 10 and 37 °C temperatures, as well as statistical analyses to both temperature and spectral shifts for all five deconvoluted signals. The first signal in this progression, namely E1 can be attributed to C-H stretching motions from PPO's CH proton. This was only observed to exhibit a small yet statistically significant increase in the pairwise comparison for the intensity on going from 10 to 37 °C. Along those lines, E4-5 are also associated to vibrational motions within the PPO segments. However, unlike E1 these are related to symmetric and asymmetric methyl C-H vibrational motions, respectively. In both cases and similarly to E1, we report statistically significant increase in their intensities, which can be structurally associated to an increase in the order of these units in the nuclei of the formed micelles. This structural re-arrangement at molecular level is further denoted by the lower frequency shift as a function of temperature, particularly in the case of the asymmetric vibration in E4, as illustrated in **Figure 5**. The transition of PPO segments to a central position on micellization decreases the intermolecular interactions with surrounding water molecules, hence leading to a decrease in the vibrational frequencies for these motions. PEO associated vibrational bands, E2-3 are in turn characterised by an increase in their vibrational frequencies as a result of the thermally-induced process ( $\bar{\nu} = 2889.4/2890.7$  and  $2924.3/2926.3$   $\text{cm}^{-1}$  for E2/E3 at 10 and 37 °C, respectively). Unlike the molecular events described for PPO units as a result of temperature increase in these P407 aqueous formulations, PEO blocks form the outer shell of the micelles. As a result, the increase in the vibrational frequencies can be associated to strengthened intermolecular interactions with water molecules upon micellization. This also mean that PEO units adopt a less ordered structure as the temperature is increased in these systems. The latter is evidenced spectrally by the decrease in the intensity of E2. In this regard, it was somehow of surprise to us the opposite behaviour exhibited by the band associated to the symmetric stretching motion, E3 which increases the intensity as a function of temperature. Firstly, we attribute the latter to a comparably large uncertainty associated to the intensities at 37 °C. To further shed light into this observation, we went on to compute the intensity ratios, defined as PEO/PPO, for these symmetric (E2/E4) and asymmetric (E3/E5) vibrational modes. We observed, in both cases, that the PEO/PPO ratios exhibit statistically significant decreases

as the temperature of the formulations was increased, thus consistent with a greater thermally-induced disorder in the case of the PEO units located in the outside of the micelles.

In light of this observations and our hypothesis that the vibrational implications of these thermally induced processes should not be restricted to the analysis of C-H stretching modes, next we evaluated in-depth the remaining four key spectral regions for any markers that could further aid in monitoring such processes by Raman spectroscopy.

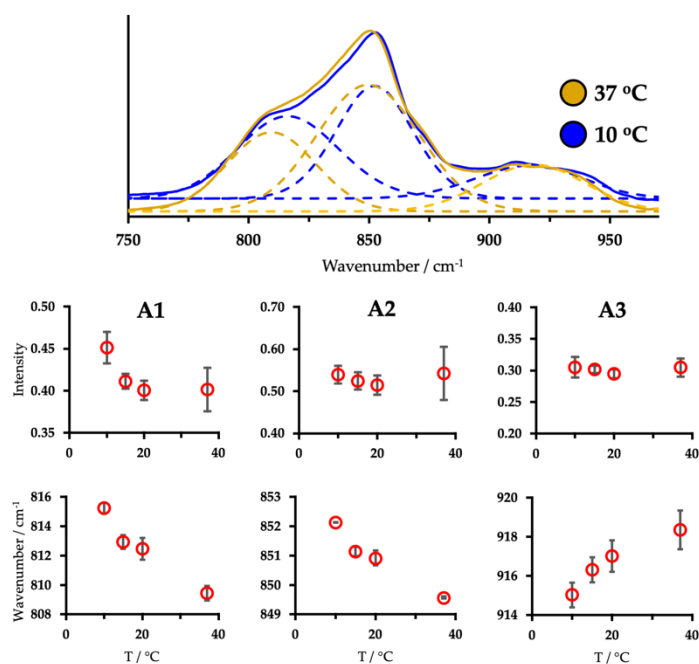


**Figure 6.** Raman spectra of 20% w/w aqueous formulations of P407 at 10 (blue solid line) and 37 °C (yellow solid line), including deconvoluted bands (illustrated as dotted lines) for the A spectral region (745-972  $\text{cm}^{-1}$ ). Two dimensional Figures illustrate the changes to intensities (top) and vibrational frequencies (bottom) as a function of temperature for all deconvoluted signals (grey solid lines illustrate the associated uncertainties as standard deviations).

Region A, which extends from 745 to 972  $\text{cm}^{-1}$  and can be broadly associated to C-O-C vibrational motions<sup>[37,38]</sup> that are highly coupled to C-H rocking, was successfully deconvoluted into three different Gaussian peaks. These, namely A1-3, are centred at ca 814, 850 and 917  $\text{cm}^{-1}$ , respectively. Aided by quantum mechanical calculations, the two first of these individual vibrational bands can be associated to poloxamer's PPO units. In turn, the deconvoluted band centred at 917  $\text{cm}^{-1}$  can be associated to PEO units. Visual inspection of this spectral region in the convoluted spectra in **Figure 2** was anticipated to be consistent with an increase in the intensity of the shoulder signal, at lower frequency with respect to the most intense band, with

temperature. However, following careful spectral deconvolution of this progression as well as statistical analysis of the variance and Tukey's post-hoc test to evaluate all possible pairwise comparisons, we report a statistically significant decrease in both intensity and frequency of the first deconvoluted signal as a function of temperature (**Figure 6**). In fact, the earlier observation can be accounted for on the basis of A2 and not A1. The former, which dominates this vibronic envelope and is also associated to PPO units in P407, shifts to lower frequencies as the temperature is increased. These observed spectral shifts to the deconvoluted signals associated to PPO segments ( $\bar{\nu} = 815.2/852.1$  and  $809.4/849.6 \text{ cm}^{-1}$  for A1/A2 at 10 and 37 °C, respectively), are consistent with reduced intermolecular interactions of these hydrophobic units with water molecules when micelles are formed with PPO in their core surrounded by hydrophilic PEO segments. In addition, the more restricted flexibility of these motifs in the micelles is also anticipated to contribute to this observation. On the contrary, the latter (A3) is characterised by a shift to higher frequencies as a function of temperature. This can be ascribed to their outer location in these thermally-generated micelles, hence preserving or even increasing the strength of the interaction with surrounding water molecules. It is of note that unlike the behaviour of the signals associated to PPO units in the E spectral region, A1 exhibits a statistically significant intensity decrease on progression from 10 °C to other interrogated temperatures (**Figure 6**). This can be accounted for on the basis of the differences in the nature of these vibrational motions and not on an increased disorder of the centrally located hydrophobic PPO units. Intensity changes as a function of temperature for A2 and A3 were observed to be non-significant.

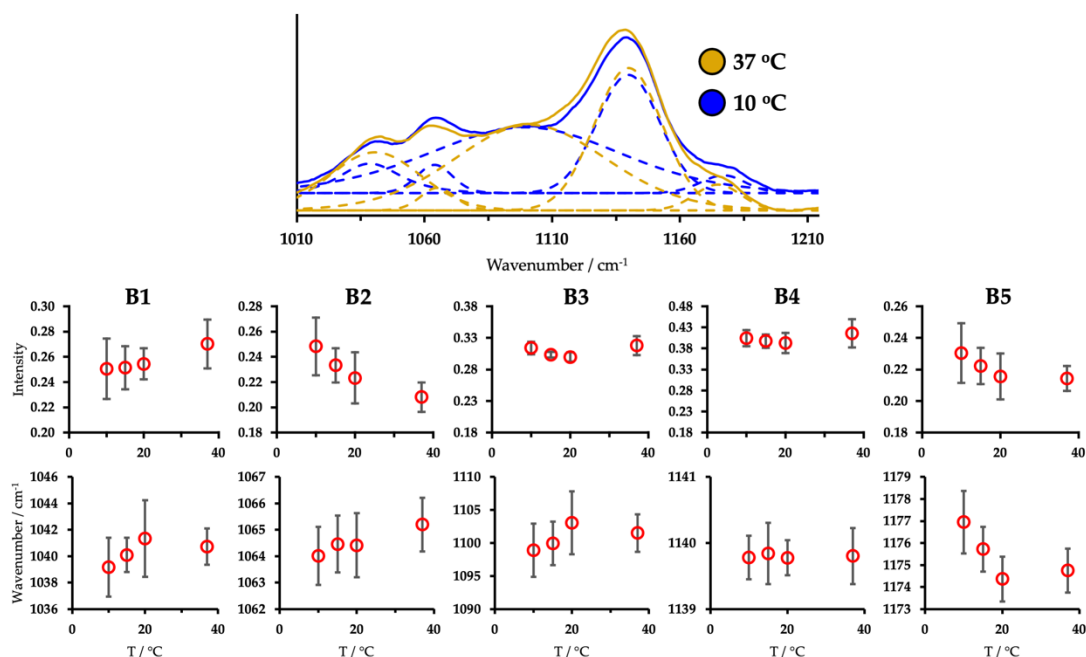


**Figure 7.** Raman spectra of 20% w/w aqueous formulations of P407 at 10 (blue solid line) and 37 °C (yellow solid line), including deconvoluted bands (illustrated as dotted lines) for the B spectral region (1010-1215  $\text{cm}^{-1}$ ). Two dimensional Figures illustrate the changes to intensities (top) and vibrational frequencies (bottom) as a function of temperature for all deconvoluted signals (grey solid lines illustrate the associated uncertainties as standard deviations).

The vibronic progression in region B is dominated by a band centred at ca 1143  $\text{cm}^{-1}$  and has a number of inflections both at lower and higher frequencies. As a result, it makes for a complex envelope and its deconvolution required five individual components, as illustrated in **Figure 7**. Following statistical analyses, we report negligible temperature-induced changes in the frequency of those vibrations, except for B5. This observation can be related to the broad nature of these bands and large associated uncertainties. The highest frequency signal (E5), which can be associated to hydrophobic PPO units, is characterised by a decrease in its frequency as the temperature is increased. Hence consistent with a diminish of the intermolecular interactions with surrounding water molecules as these units gradually re-arranged to a central location within the micelles. Although signals B1 and B3-4, which are associated to hydrophilic PEO blocks, exhibit an increase in their intensities as temperature progresses to 37 °C, these changes were observed to be non-statistically significant in all cases. Interestingly, both signals associated to PPO units, namely B2 and B5, are characterised by a statistically significant diminishment of their intensities for those pairwise comparisons involving 10 and 37 °C. This, contrary to previously accepted understanding and along the same lines discussed for PPO

signals in the A region, would be consistent with a progression to greater disorder in the hydrophobic PPO units as a consequence of temperature. Instead, we ascribe this to the different nature of this vibrational mode and not changes to the understood molecular level mechanism of these thermally-induced processes.

Next, we evaluated the changes as a function of temperature to the spectral signatures in regions C and D, broadly associated to C-H wagging/rocking and bending vibrational motions, respectively. The first of these vibrational envelopes can be successfully deconvoluted into three different Gaussian bands, centred at ca 1249, 1286 and 1309  $\text{cm}^{-1}$ , referred to in the following as C1-3, respectively. While the first of these three signals can be associated to central PPO units, C2-3 are assigned to terminal regions of the hydrophilic PEO segments. We observe that in line with the behaviour identified in other key spectral regions, the vibrational frequencies associated to PPO/PEO units are characterised by a decrease/increase as a function of temperature (**Figure 8**). In all cases these shifts were observed to be above the resolution of our instrument of choice and statistically significant for pairwise comparisons involving formulations at  $T = 10$  and  $37$  °C. In turn, a different scenario was observed for intensity changes in these deconvoluted signals. In short, whilst the progression is dominated by the central, C2 band, intensity changes were most significant in the case of C3 which denotes an inflection to the main vibrational component. This, associated to PEO units in P407, was observed to exhibit a significant diminish in intensity as the temperature increased. Thus, consistent with the structural re-arrangements of these hydrophilic units to the outer region of the thermally-generated micelles and their transition to a more disordered state.

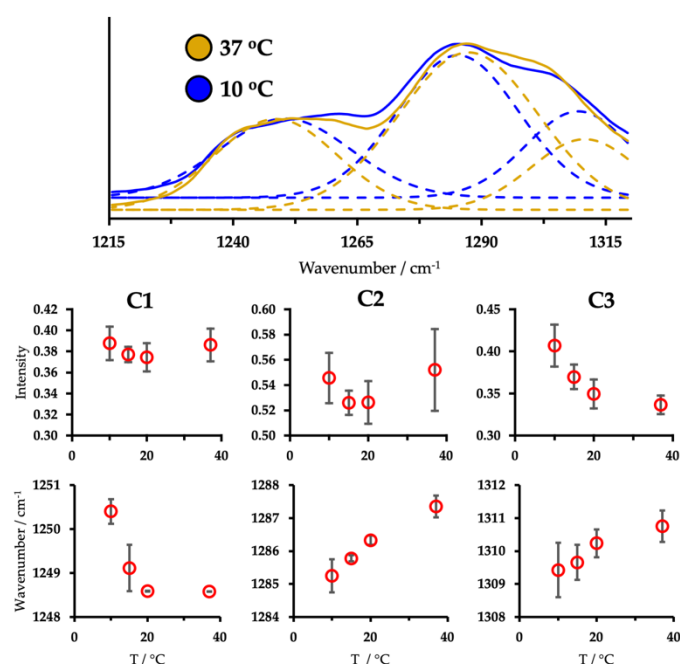


**Figure 8.** Raman spectra of 20% w/w aqueous formulations of P407 at 10 (blue solid line) and 37 °C (yellow solid line), including deconvoluted bands (illustrated as dotted lines) for the C spectral region (1215-1320 cm<sup>-1</sup>). Two dimensional Figures illustrate the changes to intensities (top) and vibrational frequencies (bottom) as a function of temperature for all deconvoluted signals (grey solid lines illustrate the associated uncertainties as standard deviations).

Region D, in line with the arguably small spectral range (1430-1500 cm<sup>-1</sup>), only required two Gaussian bands to achieve a successful deconvolution. D1 and D2, centred at ca 1455 and 1475 cm<sup>-1</sup>, can be associated to PPO and PEO units respectively. Similarly to the scenario described for the previous spectral region (C), negligible intensity changes were observed for the signal (D2) that dominates the progression, also associated to corona PEO blocks. In this regard, it was previously anticipated that an increase in the temperature in these aqueous formulation results in a relatively higher intensity of the lower frequency inflection. This observation was confirmed following the spectral deconvolution of this envelope, which is consistent with a statistically significant increment of D1 whilst intensity changes to D2 were negligible. This finding is in agreement with current mechanistic understanding of these systems at the molecular level for vibrational motions involving hydrogen atoms. Hydrophobic PPO units undergo a thermally-controlled decrease in their structural disorder as they are structurally restricted in the core of the formed micelles. In addition, as a consequence of this process they reduce their intermolecular interactions with surrounding water molecules. The latter is

supported by the observed diminish of the vibrational frequency of D1 ( $\bar{\nu} = 1456.5$  and  $1455.0$   $\text{cm}^{-1}$  at  $10$  and  $37$   $^{\circ}\text{C}$ , respectively) which further contributes to the visual aspect of the convoluted band in **Figure 9**.

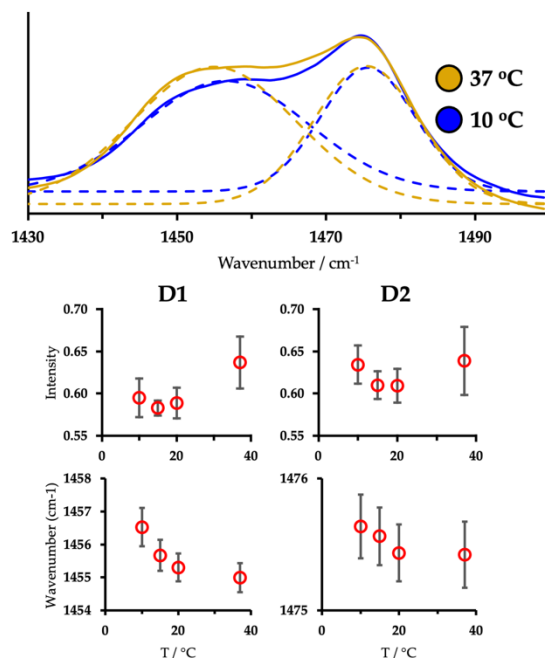


**Figure 9.** Raman spectra of 20% w/w aqueous formulations of P407 at  $10$  (blue solid line) and  $37$   $^{\circ}\text{C}$  (yellow solid line), including deconvoluted bands (illustrated as dotted lines) for the D spectral region ( $1430$ - $1500$   $\text{cm}^{-1}$ ). Two dimensional Figures illustrate the changes to intensities (top) and vibrational frequencies (bottom) as a function of temperature for all deconvoluted signals (grey solid lines illustrate the associated uncertainties as standard deviations).

As a result, we have extensively demonstrated that the evaluation and monitoring of molecular level re-arrangements following these thermally-induced processes in 20% w/w P407 aqueous formulations should not be restricted to spectral signatures associated to C-H vibrational motions. In addition, our results are consistent with the necessity to analyse deconvoluted bands. We strongly believe that limiting spectral interpretation to complex convoluted envelopes can often lead to misconceptions, given that the overall behaviour might not be determined by signals located at the centre of the progression. It is also of note that entropic effects to building blocks as a function of temperature can have varying vibrational behaviour depending on the spectral region being evaluated. It is anticipated that this can bear important implications in the development of algorithms for real-time monitoring of micellization processes employing spectroscopic techniques.

#### 4. Conclusions

In this work we carry out an in-depth evaluation of thermally-induced processes in 20% w/w P407 aqueous formulations by means of Raman spectroscopy coupled to computational techniques. Previous efforts on structural analogues were consistent with arguably clear spectral changes associated to C-H vibrational motions. In turn, herein we conclude that supramolecular re-arrangements in P407 should not be restricted to that spectral region. In fact, aided by chemometric approaches by principal components, we identified optimum delineation of formulations at different temperatures is achieved by utilising the full spectral dataset and not individual regions of interest. In addition, we observed this delineation to be consistent with a gradual shift in equilibria towards micelles formation, rather than a rapid transition onset to an entirely micellar state. This was further confirmed by means of rheological as well as dynamic light scattering analyses. Next, we went on to deconvolute these complex vibrational envelopes into their individual contributions for all key spectral regions, A-E. These were then associated to particular polymer building blocks by means of quantum mechanics calculations on a P407 representative enneadecamer. Changes to both intensity and vibrational frequencies were statistically evaluated and rationalised based on structural re-arrangements of the different polymer building blocks, namely PEO and PPO. It is of note that inspection of the convoluted spectra can result in misinterpretations of the structural re-arrangements in these thermally-induced processes and therefore spectral deconvolution is critical. We observed that for vibrational signatures involving H atoms in the polymer structure, such as C-H stretching, rocking and bending motions, there is a decrease/increase of the intensity of the band as well as a spectral shift to higher/lower frequencies as a function of temperature, for PPO/PEO units. These observations can be rationalised based on i) the progression of hydrophobic PPO segments occupying the centre of the micelles to a more ordered structure and as a result a diminish of the intermolecular interactions with water molecules as well as ii) the PEO units occupying the outer region of these micelles undergoing a transition to a more disordered state with increasing interactions with surrounding water molecules. It is known that PEO chains form clusters in solution,<sup>[39]</sup> and a hypothesised mechanism for this observation would be that PEO-PEO or PPO-PEO interactions in these clusters break down at lower temperatures than H-bonds hydrating the chains, though further analysis is required. Furthermore, the precise nature of order vs disorder in these systems can be further expanded from the semi-qualitative paradigm adopted in this study. Interestingly and contrary to previous misconceptions, spectral signatures on progression to a micellar state are somehow different for spectral features

associated to vibrational motions, such as C-O-C stretching. In this regard, such observations which particularly affect spectral signatures associated to PPO units, can be rationalised based on the different nature of the vibrational motion and not a change in the mechanism of micellization. As a result, we anticipate this work to be of interest to the growing community of polymer scientists interested in real-time monitoring of micellization processes as well as those devoted to the realisation of superior technologically-relevant polymer materials to those currently exploited.

### Supporting Information

Supporting Information is available from the Wiley Online Library. S1, two-dimensional score plots for all key spectral regions evaluated; S2, line loading plots for all generated PCA models; S3, optimized geometry for the representative P407 enneadecamer.

### Acknowledgements

MTC would like to thank the EPSRC EP/T00813X/1 for funding his research on thermoresponsive materials. The University of Hertfordshire are acknowledged for funding the PhD programme of MAA-S

### Data Availability Statement

Data is available from the authors upon reasonable request.

**Received:** ((will be filled in by the editorial staff))

**Revised:** ((will be filled in by the editorial staff))

**Published online:** ((will be filled in by the editorial staff))

### 4. References

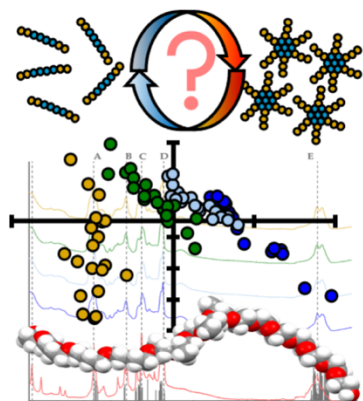
- [1] M. T. Cook, P. Haddow, S. B. Kirton, W. J. McAuley, *Advanced Functional Materials* **2021**, *31*, 2008123.
- [2] M. S. H. Akash, K. Rehman, *Journal of Controlled Release* **2015**, *209*, 120.
- [3] L. Mi, H. Xue, Y. Li, S. Jiang, *Advanced Functional Materials* **2011**, *21*, 4028.
- [4] M. Müller, J. Becher, M. Schnabelrauch, M. Zenobi-Wong, *Biofabrication* **2015**, *7*.
- [5] M. A. Ward, T. K. Georgiou, *Polymers* **2011**, *3*, 1215.
- [6] M. A. Abou-Shamat, J. Calvo-Castro, J. L. Stair, M. T. Cook, *Macromolecular Chemistry and Physics* **2019**, *0*, 1900173.
- [7] P. Haddow, W. J. McAuley, S. B. Kirton, M. T. Cook, *Mater. Adv.* **2020**, *1*, 371.
- [8] T. Gratieri, G. M. Gelfuso, E. M. Rocha, V. H. Sarmiento, O. de Freitas, R. F. V. Lopez, *European Journal of Pharmaceutics and Biopharmaceutics* **2010**, *75*, 186.

- [9] M. L. Bruschi, D. S. Jones, H. Panzeri, M. P. D. Gremião, O. de Freitas, E. H. G. Lara, *Journal of Pharmaceutical Sciences* **2007**, *96*, 2074.
- [10] M. A. Abou-Shamat, J. L. Stair, S. B. Kirton, J. Calvo-Castro, M. T. Cook, *Mol. Syst. Des. Eng.* **2020**, *5*, 1538.
- [11] K. Mortensen, Y. Talmon, *Macromolecules* **1995**, *28*, 8829.
- [12] R. K. Prud'homme, G. Wu, D. K. Schneider, *Langmuir* **1996**, *12*, 4651.
- [13] M. Valero, C. A. Dreiss, *Langmuir* **2010**, *26*, 10561.
- [14] G. Wanka, H. Hoffmann, W. Ulbricht, *Colloid & Polymer Science* **1990**, *268*, 101.
- [15] K. Mortensen, J. S. Pedersen, *Macromolecules* **1993**, *26*, 805.
- [16] P. Talik, P. Moskal, L. M. Proniewicz, A. Wesełucha-Birczyńska, *Journal of Molecular Structure* **2020**, *1210*, 128062.
- [17] M. Pastorzak, M. Kozanecki, J. Ulanski, *Polymer* **2009**, *50*, 4535.
- [18] C. Guo, J. Wang, H.-Z. Liu, J.-Y. Chen, *Langmuir* **1999**, *15*, 2703.
- [19] C. Guo, H. Liu, J. Wang, J. Chen, *Journal of Colloid and Interface Science* **1999**, *209*, 368.
- [20] A. M. Bodratti, P. Alexandridis, *Journal of Functional Biomaterials* **2018**, *9*.
- [21] I. R. Schmolka, *Journal of Biomedical Materials Research* **1972**, *6*, 571.
- [22] A. D. Becke, *Physical Review A* **1988**, *38*, 3098.
- [23] A. D. Becke, *Journal of Chemical Physics* **1993**, *98*, 5648.
- [24] C. T. Lee, W. T. Yang, R. G. Parr, *Physical Review B* **1988**, *37*, 785.
- [25] Y. Shao, L. F. Molnar, Y. Jung, J. Kussmann, C. Ochsenfeld, S. T. Brown, A. T. B. Gilbert, L. V. Slipchenko, S. V. Levchenko, D. P. O'Neill, R. A. DiStasio Jr., R. C. Lochan, T. Wang, G. J. O. Beran, N. A. Besley, J. M. Herbert, C. Y. Lin, T. Van Voorhis, S. H. Chien, A. Sodt, R. P. Steele, V. A. Rassolov, P. E. Maslen, P. P. Korambath, R. D. Adamson, B. Austin, J. Baker, E. F. C. Byrd, H. Dachsel, R. J. Doerksen, A. Dreuw, B. D. Dunietz, A. D. Dutoi, T. R. Furlani, S. R. Gwaltney, A. Heyden, S. Hirata, C.-P. Hsu, G. Kedziora, R. Z. Khalliulin, P. Klunzinger, A. M. Lee, M. S. Lee, W. Liang, I. Lotan, N. Nair, B. Peters, E. I. Proynov, P. A. Pieniazek, Y. M. Rhee, J. Ritchie, E. Rosta, C. D. Sherrill, A. C. Simmonett, J. E. Subotnik, H. L. Woodcock III, W. Zhang, A. T. Bell, A. K. Chakraborty, D. M. Chipman, F. J. Keil, A. Warshel, W. J. Hehre, H. F. Schaefer III, J. Kong, A. I. Krylov, P. M. W. Gill, M. Head-Gordon, *Physical Chemistry Chemical Physics* **2006**, *8*, 3172.
- [26] A. Szabo, N. S. Ostlund, *Modern Quantum Chemistry: Introduction to Advanced Electronic Structure Theory*, McGraw-Hill, **1989**.
- [27] F. Jensen, *Introduction to computational chemistry* (Ed.: sons, J. W. and), John Wiley and sons, **2007**.
- [28] I. M. Alecu, J. Zheng, Y. Zhao, D. G. Truhlar, *Journal of Chemical Theory and Computation* **2010**, *6*, 2872.
- [29] The National Institute of Standards and Technology (NIST), *Computational Chemistry Comparison and Benchmark DataBase, Release 21*, The National Institute of Standards and Technology (NIST), **2020**.
- [30] E. Smith, G. Dent, *Modern Raman Spectroscopy. A Practical Approach*, John Wiley & Sons, Ltd., **2005**.
- [31] Y. Su, J. Wang, H. Liu, *Langmuir* **2002**, *18*, 5370.
- [32] B. Li, A. Calvet, Y. Casamayou-Boucau, C. Morris, A. G. Ryder, *Analytical Chemistry* **2015**, *87*, 3419.
- [33] J. Calvo-Castro, A. Guirguis, E. G. Samaras, M. Zloh, S. B. Kirton, J. L. Stair, *RSC Adv.* **2018**, *8*, 31924.
- [34] Z. Han, H. Liu, J. Meng, L. Yang, J. Liu, J. Liu, *Anal. Chem.* **2015**, *87*, 9500.
- [35] G. Wanka, H. Hoffmann, W. Ulbricht, *Macromolecules* **1994**, *27*, 4145.
- [36] K. te Nijenhuis, *Colloid and Polymer Science* **1981**, *259*, 1017.
- [37] S. Yoon, K. Ichikawa, W. J. MacKnight, S. L. Hsu, *Macromolecules* **1995**, *28*, 4278.
- [38] S. Yoon, K. Ichikawa, W. J. MacKnight, S. L. Hsu, *Macromolecules* **1995**, *28*, 5063.

[39] B. Hammouda, D. L. Ho, S. Kline, *Macromolecules* **2004**, *37*, 6932.

## Table of Contents Entry

Michael T. Cook, Mohamad A. Abou-Shamat, Jacqueline L. Stair and Jesus Calvo-Castro\*



Understanding thermally-induced processes in aqueous formulations of P407 by means of Raman spectroscopy coupled to computational approaches